PHYSICAL ETCHING/DEPOSITION SIMULATION WITH COLLISION-FREE BOUNDARY MOVEMENT

Z. Hsiau, E. C. Kan, J. P. McVittie and R. W. Dutton

Center for Integrating Systems
Stanford University, Stanford, CA 94305

Abstract

We demonstrate that accurate and robust physical simulation of etching and deposition in the semiconductor manufacturing technology can be achieved by using the collision-free boundary movement method [1-3]. Constraints for preserving physical accuracy, treatment of multiple junctions, adaptive gridding by quad/oct-tree meshes and experimental corroboration of void and stringer formation in 2D and 3D structures will be presented.

Introduction

Physical simulation of etching and deposition in 2D and 3D has become increasingly important for both front-end device and back-end interconnect modeling. To account for the effects from complex geometry and selection of various etching and deposition processes, an accurate and robust boundary movement method is indispensable. Not only that successive simulation steps need entirely valid geometry representations (no loop formation), but also the accuracy in growth rate calculation will be lost if *ad hoc* boundary movement steps are taken for convenience. Traditionally boundary movement is based on motion of discretized surface mesh or nodal envelopes [4]. It suffers from topological degeneration due to boundary collision and shock formation, which is marginally tractable for 2D boundaries (topological 1D) and almost impossible for 3D. The cell method for boundary movement also has difficulties in boundary curvature evaluation to calculate physical growth rates [4]. A collision-free boundary movement method based on the level-set approach [1-3] has been implemented in the physical etching/deposition simulator SPEEDIE for both 2D and 3D cases [5]. It will be shown that the closure of two boundaries and the triple-point problem in multiple-junction movement can be correctly modeled in a *physical* way. Adaptive gridding with quad/oct-tree based meshes in the Eulerian interface representation will be also presented.

Boundary Movement Calculation

As an example in 2D (extension to 3D is listed in Fig. 1), the level-set function $\psi(x,y)$ can be conveniently defined as a function of the signed distance from the point (x,y) to the boundary being considered. The boundary movement can then be modeled by

$$\psi_t + \frac{\partial\psi}{\partial x}\frac{\partial x}{\partial t} + \frac{\partial\psi}{\partial y}\frac{\partial y}{\partial t} = 0 \qquad (1)$$

The contour of $\psi = 0$ at different time steps defines the moving 2D surface. Notice that the boundary collision is taken into consideration naturally without additional topological validation. The possible boundary collision can be tracked by $\nabla\psi|_{(x,y)} = 0$, with $\nabla^2\psi < 0$ for collision of outside boundaries (merge) or $\nabla^2\psi > 0$ for collision of inside boundaries (cutoff). Additional conservation laws will be required to solve (1) correctly. Hence, the physical etching/deposition quantity Q (molecules/cm^2) calculated from SPEEDIE are used to preserve accurate volume expansion or depletion in consideration of curvature:

$$\begin{aligned} \psi(t+\Delta t) &= \psi(t) - L(Q,K,\rho)\,|\nabla\psi| && (2) \\ L(Q,K,\rho) &= \frac{2Q}{\rho\left(\sqrt{1+2KQ/\rho}+1\right)} && (3) \\ K &= \frac{\psi_{yy}\psi_x^2 - 2\psi_x\psi_y\psi_{xy} + \psi_{xx}\psi_y^2}{(\psi_x^2+\psi_y^2)^{3/2}} && (4) \end{aligned}$$

where K is the curvature (μm^{-1}) and ρ is the density (molecules/μm-cm^2). $L \to Q/\rho$ as $K \to 0$. To retain the accuracy of Q, the following constraints will apply in analogy to the natural growth of molecule layers:

$$\begin{aligned} Q &> -\rho/2K \quad \text{if } K > 0 && (5) \\ Q &< -\rho/2K \quad \text{if } K < 0 && (6) \end{aligned}$$

The curvature K can be very large close to merge or split of boundaries, where the etching/deposition rate constrained by (5) and (6) may become unnecessarily small. A lower limit can be imposed so that there is at least one molecule etched or deposited in a given surface element during the time step.

Examples

Figure 2 shows the evolution of deposition for an overhang structure. The deposition rate is calculated using SPEEDIE with anisotropic ion enhancement and with a neutral flux of a sticking coefficient of 0.01. Figure 2(b) compares well with the SEM picture in Fig. 3. As the deposition continues, Fig. 2(c) shows the merging of two boundaries and 2(d) the inside void formation and planarization on the top surface. Grid adaptation is shown in Figs. 4 and 5 and will be discussed in the last section. Figure 6 demonstrates the 3D simulation of stringer formation during poly-silicon etch. A blanket of poly is deposited on the nonflat surface, and then the anisotropic plasma etch is applied for the 2-poly-line mask. Stringers may be formed and short the two poly lines if the overetch time is not long enough. With the reduction in line width, underlying steps can become steeper and the gate oxide become thinner. Control of stringer formation becomes more critical. Figure 7 shows the cross section on the dashed line in Fig. 6(d), and the stringer shape compares well with the SEM picture in [6]. Figures 8 and 9 show the result of an isotropic etch, where the boundary movement velocity is only a function of curvature but not the ion flux, stringers will also be formed after the central poly disappears since the curvature will enhance or decrease the deposition and etch rate differently.

Multiple Regions and Triple Points

Multiple region movement, as in the so-called triple point for silicon-oxide-nitride interface, is very hard to be modeled correctly by surface mesh and nodal motion, since the progression of the triple point will require node and mesh splits. However, it is much easier to use the collision-free method to track this multiple-junction movement by additional level set functions defined with respect to each material boundary [7]. Each boundary is first moved separately and then adjusted according to

$$\psi_i = \psi_i - \max_{j \neq i} \psi_j \ . \qquad (7)$$

The triple-point movement is illustrated in Fig. 10. To use the rate Q from SPEEDIE, however, a global surface level set function is more accurate. Individual material level set functions will adjust to the global function at each time step. Physical etching simulation with 10-to-1 selectivity is shown in Fig. 11.

Adaptive Gridding

Since the boundary is defined at $\psi = 0$ in the level-set boundary movement method, accurate evaluation of small $|\psi|$ is most critical to preserve the accuracy in rate calculation. A simple algorithm of adaptive gridding can be established by recursive refinements of elements satisfying

$$A > |\bar{\psi}|^2 \ \text{ and } A > \text{MinimumAreaAllowed} \qquad (8)$$

where A is the element area. Adaptation of quad mesh for the overhang structure according to (8) is shown in Figs. 4 and 5. Adaptive gridding based on error analysis of both ψ and Q calculated from Lagrangian and Eulerian representations of boundary remains under investigation [8]. Computational efficiency can only be marginally improved by the narrow-band method [2] owing to the adaptation of quad/oct-tree mesh. Nevertheless, in the present implementation, the boundary movement algorithm has taken less than 5% of the time for physical Q calculation.

Acknowledgement

This work is supported by ARPA under contract DABT63-93-C-0053. The authors wish to thank Prof. Neureuther of UC Berkeley for allowing access to SAMPLE-3D to evaluate 3D string and cell methods, and Prof. Sethian also of UC Berkeley for helpful discussions.

Reference

[1] S. Osher and J.A. Sethian, "Fronts propagating with curvature-dependent speed: algorithms based on Hamilton-Jacobi formulations," *J. Comp. Phys.*, vol. 79, pp. 12-49, 1988.

[2] R. Malladi, J.A. Sethian and B.C. Vemuri, "Shape modeling with front propagation: a level set approach," *IEEE Trans. Patt. Anal. Mach. Intell.*, vol. 17, pp. 158-174, 1995.

[3] D. Adalsteinsson and J. A. Sethian, "A level set approach to a unified model for etching, deposition, and lithography I: algorithms and two-dimensional simulations," *J. Comp. Phys.*, vol. 120, pp. 128-144, 1995.

[4] A.R. Neureuther, et. al., "3D Topography simulation using surface representation and central utilities," *3-dimensional Process Simulation*, ed. J. Lorenz, New York: Springer-Verlag, 1995, p. 57.

[5] J.P. McVittie, et. al., *SPEEDIE User's Manual*, Stanford University, Aug. 1995.

[6] B. Haselden, P. Peavey and B. Elicson, "Profile control and stringer removal during plasma etch of submicron meter polysilicon lines, " *SPIE Dry Proc. Submicron. Litho.*, vol. 1185, pp. 115-127, 1989.

[7] B. Merriman, J.K. Bence and S.J. Osher, "Motion of multiple junctions: a level set approach," *J. Comp. Phys.*, vol. 112, pp. 334-363, 1994.

[8] D.J. Benson, "Computational methods in Lagrangian and Eulerian hydrocodes," *Computer Methods in Appl. Mech. Engr.*, vol. 99, pp. 235-394, 1992.

$$\boxed{\begin{array}{ll}
\text{If } K \cdot Q > 0, & \rho L + \rho K^2 L^3/3 = Q \\
 & L \text{ is between } 0 \text{ and } Q/\rho \\
\text{If } K \cdot Q < 0, & \rho L - \rho K^2 L^3/3 = Q \\
 & L \text{ is between } -|1/K| \text{ and } |1/K| \\
 & \text{if } Q > 0,\ Q < 2\rho/3|K| \\
 & \text{if } Q < 0,\ Q > -2\rho/3|K| \\
\multicolumn{2}{l}{K \text{ is chosen as the mean curvature [6] and is}} \\
 & \text{in unit of } \mu m^{-1}.
\end{array}}$$

Fig. 1: Equations for 3D boundary movement calculation.

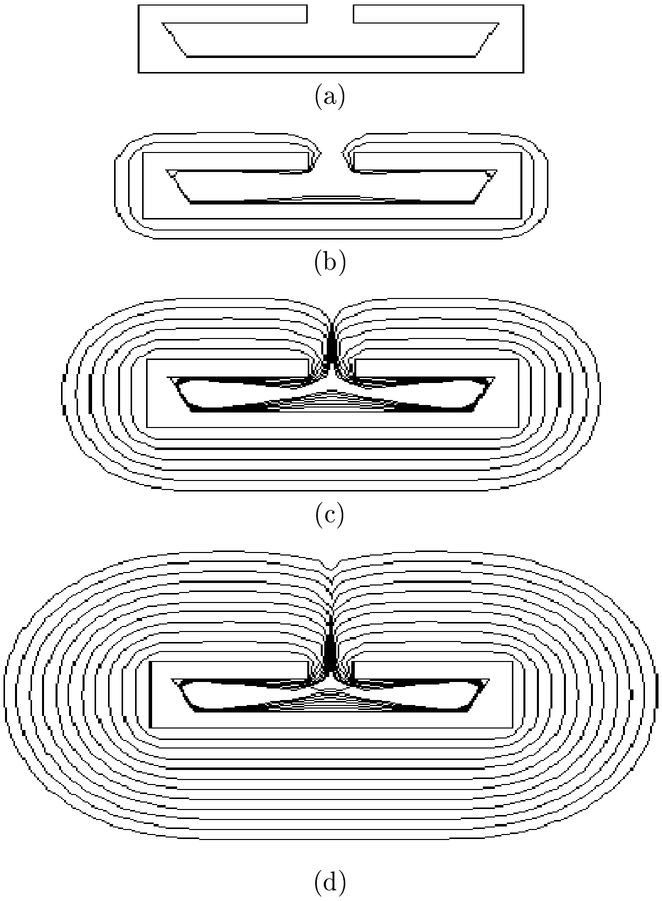

Fig. 2: Boundary evolution for PECVD of an overhang structure.

Fig. 3: An SEM picture showing PECVD (middle layer) in Fig. 2(b).

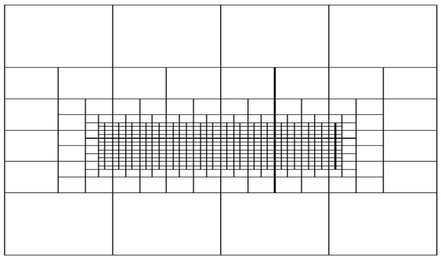

Fig. 4: Starting quad mesh adapted to the geometry in Fig. 2(a).

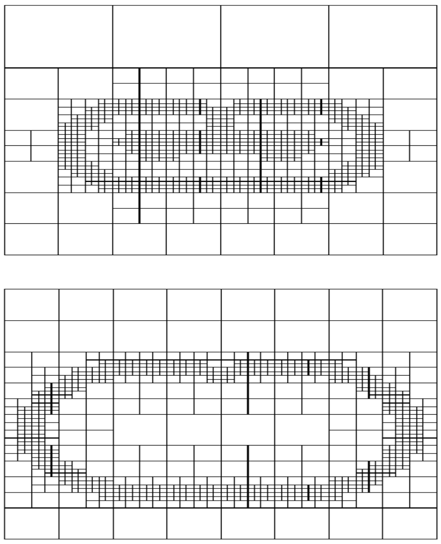

Fig. 5: quad mesh adapted to the geometry in Fig. 2 (c) and (d).

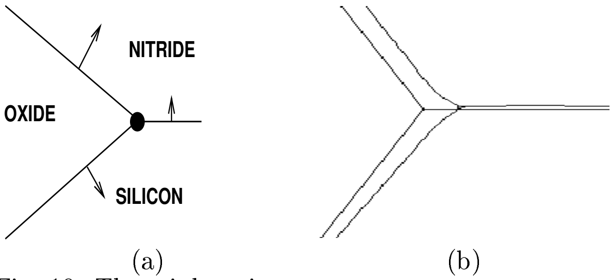

Fig. 10: The triple-point movement.

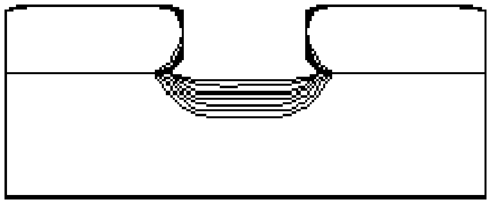

Fig. 11: Etching simulation with multiple regions.

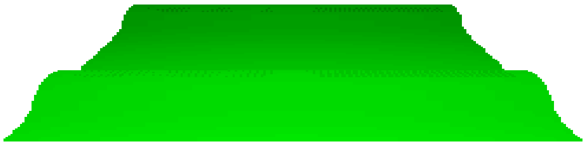

(a)

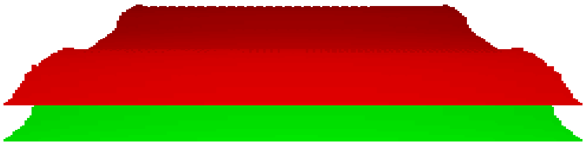

(b)

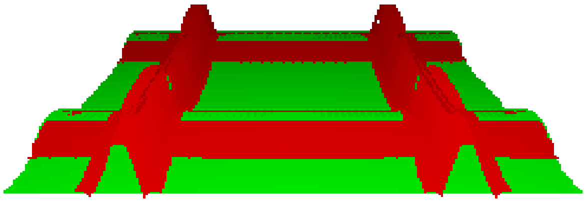

(c)

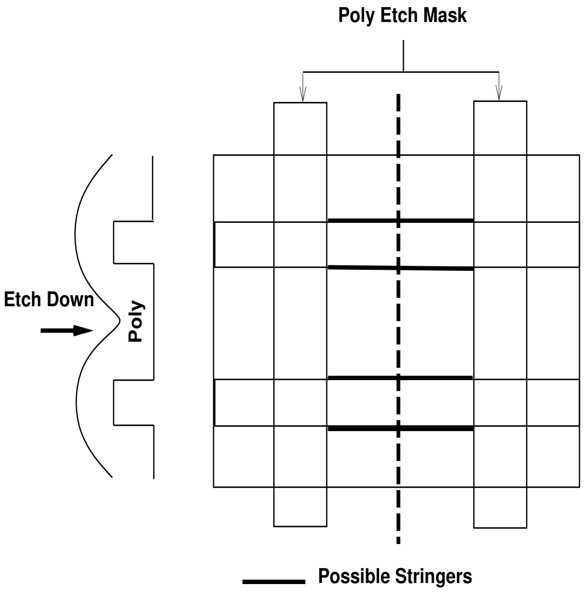

(d)

Fig. 6: Surface mesh plots of stringer formation.

(a)

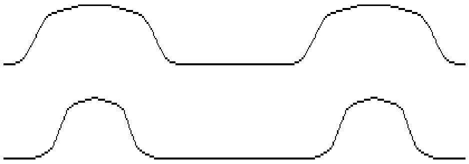

(b)

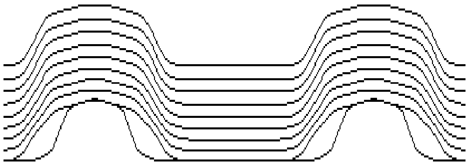

(c)

(d)

Fig. 7: Cross section at the center dashed line in Fig. 6(d). Figs. 7(a) to (c) show surface progression and (d) shows the final stringers.

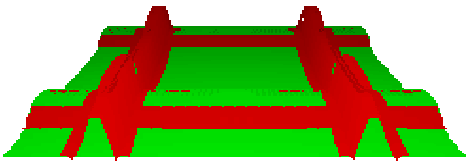

Fig. 8: Final results of isotropic etch.

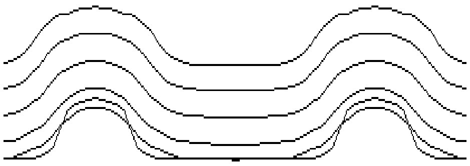

Fig. 9: Cross section of Fig. 8.